CRUICKSHANK, E., STRACHAN, G.J., STOREY, J.M.D. and IMRIE, C.T. 2022. Chalcogen bonding and liquid crystallinity: understanding the anomalous behaviour of the 4'-(alkylthio)[1,1'-biphenyl]-4-carbonitriles (nSCB). *Journal of molecular liquids* [online], 346, article 117094. Available from: https://doi.org/10.1016/j.molliq.2021.117094

Chalcogen bonding and liquid crystallinity: understanding the anomalous behaviour of the 4'-(alkylthio)[1,1'-biphenyl]-4-carbonitriles (nSCB).

CRUICKSHANK, E., STRACHAN, G.J., STOREY, J.M.D. and IMRIE, C.T.

2022

Supplementary materials are appended after the main text of this document.

OpenAIR @RGU

This document was downloaded from https://openair.rgu.ac.uk

CC BY NC ND

Chalcogen bonding and liquid crystallinity: Understanding the anomalous behaviour of the 4′-(alkylthio)[1,1′-biphenyl]-4-carbonitriles (*n*SCB)

Ewan Cruickshank, Grant J Strachan, John MD Storey, Corrie T Imrie *

Department of Chemistry, School of Natural and Computing Sciences, University of Aberdeen, Meston Building, Aberdeen AB24 3UE, UK

* Corresponding author. *E-mail address:* c.t.imrie@abdn.ac.uk (C.T Imrie).

A B S T R A C T

The synthesis and characterisation of the first eleven members of the 4′-(alkylthio)[1,1′-biphenyl]-4-car bonitriles series is reported. All eleven members show monotropic liquid crystal behaviour. The first six members are exclusively nematogenic, the seventh member shows nematic and smectic A phases, and the higher homologues only smectic A behaviour. A comparison of their transitional behaviour with that of the corresponding alkyl and alkyloxy-cyanobiphenyls reveals a new pattern of behaviour. Specifically, the nematic-isotropic transition temperatures show a large decrease on passing from the methylthio to ethylthio homologues. This unexpected behaviour is interpreted in terms of chalcogen bonding.

Keywords: 4-(Alkylthio)[1,1-biphenyl]-4-carbonitriles; lkylthio; Nematic phase; Smectic A phase; Chalcogen bonding

1. Introduction

Some thirty years ago, Kato and Fréchet reported that enhanced liquid crystalline behaviour may be achieved through the formation of hydrogen-bonded complexes between different hydrogen bond acceptors and donors [1]. This seminal study triggered intense global research activity, and hydrogen bonding continues to be used extensively in the design of liquid crystals (see, for example, [2–6]). Fifteen years later, Bruce and colleagues returned to the supramolecular toolbox and used halogen-bonding to construct liquid crystal materials from dissimilar components [7]. Again, this remains a highly active area of research (see, for example, [8–12]). Both hydrogen and halogen bonding are examples of an electron donor interacting with an electrophilic region of an electron acceptor. A third type of non-covalent bond in this class of attractive interactions is the chalcogen bond [13]. It has been suggested that electrostatic interactions are dominant in the formation of chalcogen bonds between sulfur atoms, and arise because chalcogen atoms, including sulfur, have regions of both positive (r-hole) and negative electrostatic potentials on their surfaces [14]. Recently, chalcogen-bonding has been exploited in the design of supramolecular solid-state functional materials [15–17] and utilised in synthesis and in the design of catalysts [18].

Nematogens containing terminal alkylthio chains are highly topical due to their high values of birefringence arising from the highly polarisable sulfur atom (see, for example,[19–23]). Highly birefringent nematogens have the potential not only to improve liquid crystal display technology, but also have an important role to play in emerging technologies such as liquid crystal lasers and lenses. At a fundamental level, the introduction of the thio linkage is providing a demanding challenge to our understanding of the relationships between molecular structure and liquid crystalline behaviour (see, for example,[24–27]).

Here, we report the synthesis and characterisation of the 4′-(a lkylthio)[1,1′-biphenyl]-4-carbonitriles,

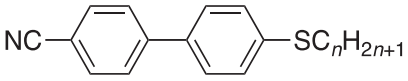

and refer to them using the acronym nSCB in which n represents the number of carbon atoms in the alkyl chain. In order to establish the effects of the thio linkage on liquid crystalline behaviour, we compare the properties of the nSCB series with those of the extensively studied 4'-(alkyl)[1,1'-biphenyl]-4-carbonitriles (nCB), and 4'-(alkyloxy)[1,1'-biphenyl]-4-carbonitriles (nOCB) [28],

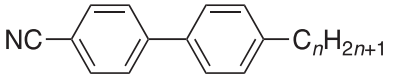

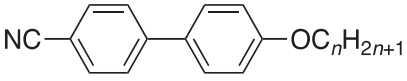

We show that the shortest members of the *n*SCB series exhibit anomalous transitional behaviour and interpret this in terms of chalcogen bonding.

2. Experimental

2.1. Synthesis

The synthetic route used to prepare the *n*SCB series is shown in Scheme 1. A detailed description of the preparation of the *n*SCB series, including the structural characterisation data for all inter-mediates and final products, is provided in the Supplementary Information.

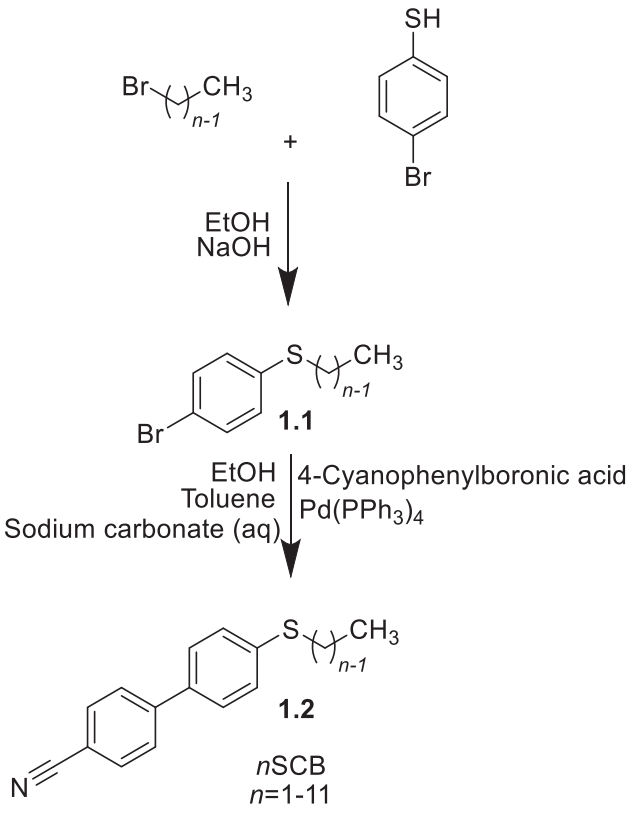

Scheme 1. Synthesis of the *n*SCB series.

2.2. Thermal characterisation

The transitional properties of the nSCB series were determined using differential scanning calorimetry using a Mettler Toledo DSC3 differential scanning calorimeter equipped with a TSO 801RO sample robot. Calibration was performed using indium as the standard. Heating and cooling rates were 10 ^{o}C min $^{-1}$ and all samples were measured under a nitrogen atmosphere. Transition temperatures and associated enthalpy changes were extracted from heating traces unless otherwise noted. For each sample, two aliquots were measured, and the data listed are the averages of the sets of data. Phase identification was performed using polarised light microscopy using an Olympus BH2 polarising opti-cal microscope equipped with a Linkam TMS 92 hot stage. All optical textures have been obtained using untreated glass slides unless stated otherwise.

2.3. Molecular modelling

Geometry optimisation was carried out using DFT calculations with Gaussian09 software.[29] Optimisation of non-sulfur com-pounds was carried out at the at the B3LYP/6-31G(d) level of theory, while the optimisation of compounds containing sulfur was performed at the at the B3LYP/6-311G(d,p) level to account for the additional electronic orbitals. Comparison of the results of optimisation for methylene- and ether-linked dimers at the B3LYP/6-311G(d,p) and the 6-31G(d) levels have been previously reported to show no discernible difference in the geometries found, so this allowed the B3LYP/6-31G(d) level to be used for the non-sulfur compounds [26]. Visualisation of electronic surfaces were generated from the optimised geometries using the GaussView 5 software, and visualisation of the space-filling and ball-and-stick models were produced post-optimisation using the QuteMol package [30].

3. Results and discussion

The transitional properties of the nSCB series are listed in Table 1. The transition temperatures for 4SCB are in excellent agreement with those reported previously [31]. The liquid crystal phases were identified on the basis of the observation of characteristic optical textures when viewed under the polarised light microscope. Specifically, for nematic phases, a schlieren texture was observed containing both two- and four-brush point singularities, see Fig. 1(a) and which flashed when subjected to mechanical stress. On cooling the nematic phase shown by 7SCB, focal conic fans developed in coexistence with homeotropically aligned regions indicative of the smectic A phase. For n > 7, on cooling the isotropic phase, focal conic fans developed and again co-existed with regions of homeotropic alignment, see Fig. 1(b), strongly suggesting a smectic A-isotropic phase transition.

All eleven members of the nSCB series exhibit monotropic liquid crystal behaviour. For n = 1–6, a nematic phase is observed, for 7SCB smectic A and nematic phases are seen, and for n > 7, nematic behaviour is extinguished and only a smectic A phase is exhibited. The dependence of the transition temperatures on the length of the alkyl chain, n, is shown in Fig. 2. The melting point falls initially on increasing n, passes through a minimum for 5SCB, and then increases gradually over the remaining members. The nematic-isotropic transition temperature, T_{NI}, falls rapidly over the first three members and then increases to 7SCB. Superimposed on this increasing trend is an alternation in which the even members exhibit the higher values. The smectic A-isotropic transition temperature, T_{SmAI}, increases without alternation over the remaining members of the series.

The transition temperatures of the nSCB series are compared with those of the nCB and nOCB series in Fig. 3. For the nCB and nOCB series, only nematic behaviour is observed for n = 1–7, smectic A and nematic phases are seen for n = 8 and 9, and the longer homologues exhibit exclusively smectic A behaviour [28,32]. In order to make meaningful comparisons between these three series, the transition temperatures for homologues having the same total chain length should be compared such that the properties of members of the nSCB and nOCB series are compared to those of the corresponding (n + 1)CB homologue. If we first consider the behaviour of the nOCB series, the values of T_{NI} show an alternation on increasing n, the so-called odd–even effect, in which the even members have the higher values. This effect attenuates on increasing, n,

Table 1
The transition temperatures and associated changes in entropy of the *n*SCB series. Cr crystal; SmA smectic A phase; N nematic phase; I isotropic phase.

n	T_{CrI} / ℃	T_{SmAN} / ℃	T_{SmAI} / ℃	T_{NI} / ℃	ΔS_{Cr} / R	ΔS_{NI} / R
1	135			78*	3.75	
2	82			53	6.34	0.19
3	63			17*	7.34	
4	64			36	7.36	0.12
5	55			27*	7.48	
6	63			43*	8.13	
7	65	37*		39*	9.29	
8	67		49*		10.79	
9	70		54*		11.69	
10	74		58*		13.32	
11	78		62*		17.28	

*Measured by microscopy.

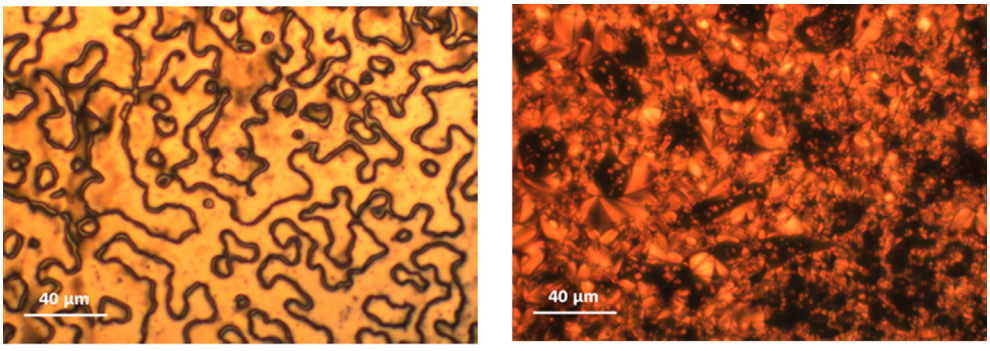

Fig. 1. The optical textures seen using polarised light microscopy for (a) the schlieren texture of the nematic phase shown by 6SCB (T = 42 ℃), and (b) the focal conic fan texture in co-existence with homeotropic regions seen for the smectic A phase for 8SCB (T = 48 ℃).

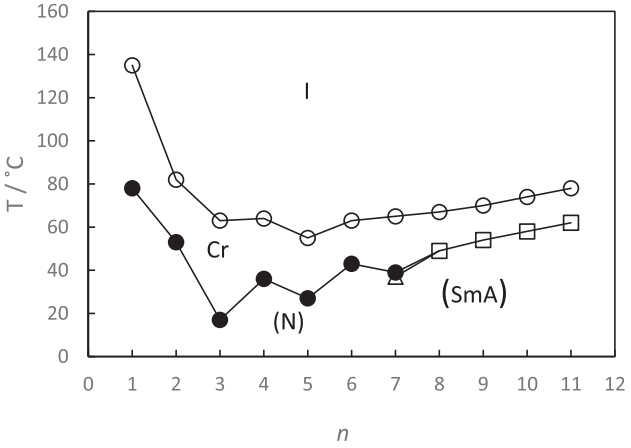

Fig. 2. The dependence of the transition temperatures of the *n*SCB series on the length, *n*, of the terminal alkylthio chain. Empty circles indicate melting points, filled circles N-I transitions, empty squares SmA-I transitions, and the empty triangle a SmA-N transition.

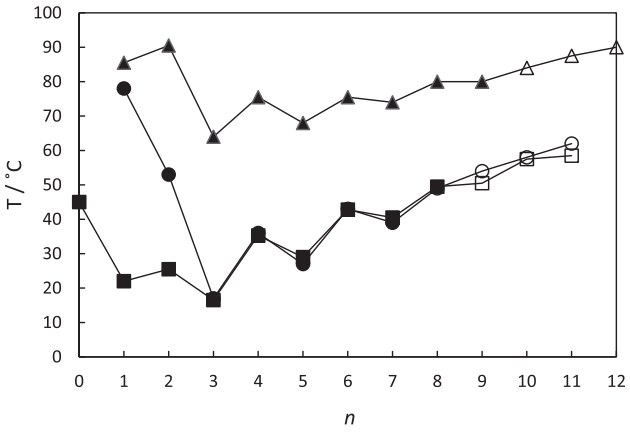

Fig. 3. The dependence of the nematic-isotropic, TNI, (filled symbols) and the smectic A-isotropic, TSmAI, transition temperatures (empty symbols) on the length of the terminal chain, n, for the nSCB (circles), nOCB (triangles) and nCB (squares) series. In order to compare similar length chains, the transition temperatures for the nCB series have been plotted against n-1.

and the values of TSmAI increase over the final three members of the nOCB series without alternation. The effect of increasing the length of a terminal chain on TNI is two-fold: first, the shape anisotropy of the molecule is enhanced increasing TNI, and second, the interactions between the mesogenic cores are diluted decreasing TNI [33]. The net effect of increasing the chain length depends on the strength of the interactions between the mesogenic cores. If the cores are large, for example three ring systems, then the dilution effect dominates and TNI falls on increasing n. Alternatively, if the cores are small, such as the two-ring systems we are considering here, then the increase in shape anisotropy dominates and TNI increases. Superimposed on this increasing trend we see an odd–even effect. This may be attributed to differences in the average shapes of molecules containing either odd- or even-membered chains. For an alkyloxy chain containing an even number of carbonatoms, the CH_2-CH_3 bond lies essentially parallel to the long axis of the mesogenic unit whereas for an odd number of carbon atoms, this bond lies at an angle to the major mesogenic unit axis. This alternation in shape is manifested in the alternation in T_{NI} [34]. Essentially identical behaviour is observed for the nCB series when plotted against (n + 1). It is striking that the dependence of the transition temperatures seen for the nSCB series deviates from this archetypal behaviour (Fig. 3). Specifically, a pronounced decrease in TNI is observed on passing from 1SCB to 2SCB rather than the anticipated increase.

The values of T_{NI} and T_{SmAI} are consistently higher for the nOCB series than for the corresponding members of the nCB series (Fig. 3). This is a wholly general observation and may be accounted for again in terms of the average shapes of these molecules. An alkyloxy chain lies more or less in-plane with the mesogenic unit it is attached to, whereas an alkyl chain protrudes at some angle (Fig. 4) [35,36]. The enhanced shape anisotropy of the former accounts for the higher T_{NI} observed. The values of T_{NI} for 1SCB and 2SCB are considerably higher than those of the corresponding members of the nCB series. Indeed, 1OCB and 1SCB show similar values of T_{NI} and some 60 C higher than that of 2CB. Adding a methylene group sees an increase in T_{NI} moving to 2OCB and 3CB but a decrease for 2SCB. Increasing the chain further, and the values of T_{NI} are essentially identical for 3SCB and 4CB and con-siderably lower than that of 3OCB. For $n \geq 3$, the clearing temperatures exhibited by the nSCB series are very similar to those seen for the corresponding members of the nCB series (Fig. 3) even though the alkylthio chain lies in the plane of the benzene ring to which it is attached [37].

We have seen that the values of TNI for 1SCB and 2SCB cannot be accounted for within the framework used to describe the dependence of TNI on the length of a terminal alkyl chain in low molarmass liquid crystals. The values of T_{NI} are considerably higher than expected for both 1SCB and 2SCB and a surprising decrease in T_{NI} is observed on passing from 1SCB to 2SCB. This unexpected fall in T_{NI} between the first and second members of an alkylthio-substituted series has been reported elsewhere but without comment[20,38]. To our knowledge, however, the nSCB series is the only complete homologous series of alkylthio-substituted compounds for which liquid crystal behaviour is observed for all the members, and in consequence, this study has revealed, for the first time, this anomalous transitional behaviour (Fig. 2). We note, however, that the anomalous behaviour has been reported for a hydrogen bonded set of materials but again without comment [39]. To account for the unexpectedly high values of T_{NI} we must invoke an additional intermolecular interaction within the nematic phase shown by 1SCB and 2SCB, and propose that this is chalcogen bonding. The chalcogen bond is a directional and attractive electrostatic interaction between regions of positive (r-hole) and negative electrostatic potentials on the surfaces of the sulfur atoms. The electrostatic potential surface for 1SCB is shown in Fig. 5 and the regions of positive and negative potential on the sulfur atom are clearly evident. An analysis of crystal structures containing cysteine fragments coupled with quantum chemical calculations on model systems revealed that parallel orientations of the two inter-acting fragments is the preferred arrangement, and that this is sta-bilised, to some extent, by the attractive r-hole interaction [14]. It would appear reasonable to assume that the orientationally ordered liquid crystal environment would also preferentially select such elongated molecular dimers as shown schematically in Fig. 6.

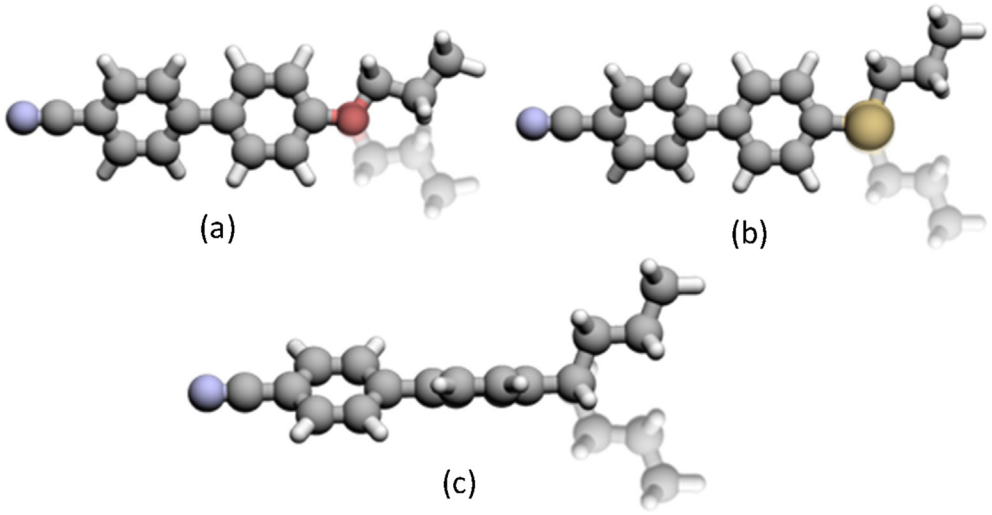

Fig. 4. A comparison of the shapes of (a) 3OCB, (b) 3SCB and (c) 4CB showing the effect of rotating about the bond between the terminal chain and the phenyl ring.

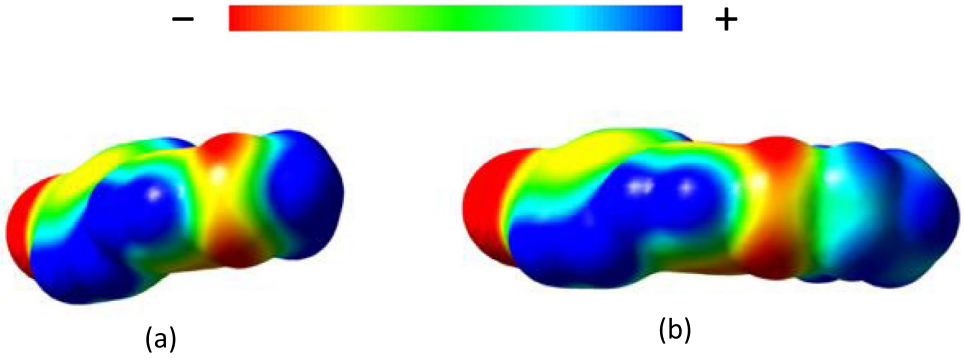

Fig. 5. The electrostatic potential surfaces for (a) 1SCB and (b) 3SCB calculated at the B3LYP/6-311G(d,p) level of theory.

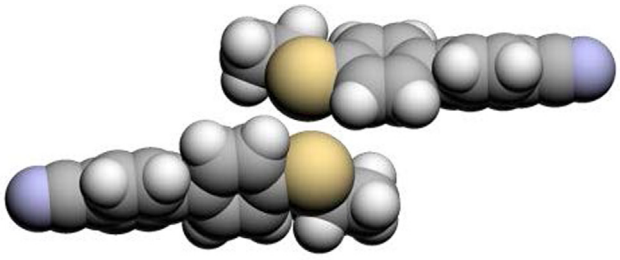

Fig. 6. An elongated molecular dimer consisting of two 2SCB molecules stabilised by a chalcogen bond.

These molecular dimers, in turn, will interact in an antiparallel fashion driven by the electrostatic interaction between the polar and polarizable cyanobiphenyl groups. In order to, at least semi-quantitatively, estimate the strength of this interaction, we calcu-lated the total energy for pairs of 1SCB, 1OCB, and 2CB molecules as a function of the distance between them, see Fig. 7(a). The energy calculations for the two interacting molecules were performed at intervals of 0.2 Å starting at 6.0 Å. The calculations were carried out at the B3LYP 6-311G(d, p) level of theory with counterpoise correction and the D3 dispersion correction [40]. These calcula-tions reveal that the 1SCB pair of molecules is the most stable of the three, and the calculated minima corresponds well to measured S-S distances. It is also apparent that these calculations reveal essentially identical total energies for the 1OCB and 2CB pairs of molecules. The molecular arrangements corresponding to the energy minima are shown in Fig. 7(b). These data strongly support the view that the chalcogen bond accounts for the much higher values of TNI seen for 1SCB and 2SCB than for their nCB counterparts.

On increasing the length of the terminal chain in the molecular dimer stabilised by chalcogen bonding (Fig. 6), the chain necessarily interacts with the biphenyl units which is entropically unfavourable, and also prevents the interaction between the cyanobphenyl units. In addition, the differing regions of electrostatic potential on the sulfur atom become less well defined as shown for 3SCB (Fig. 5).

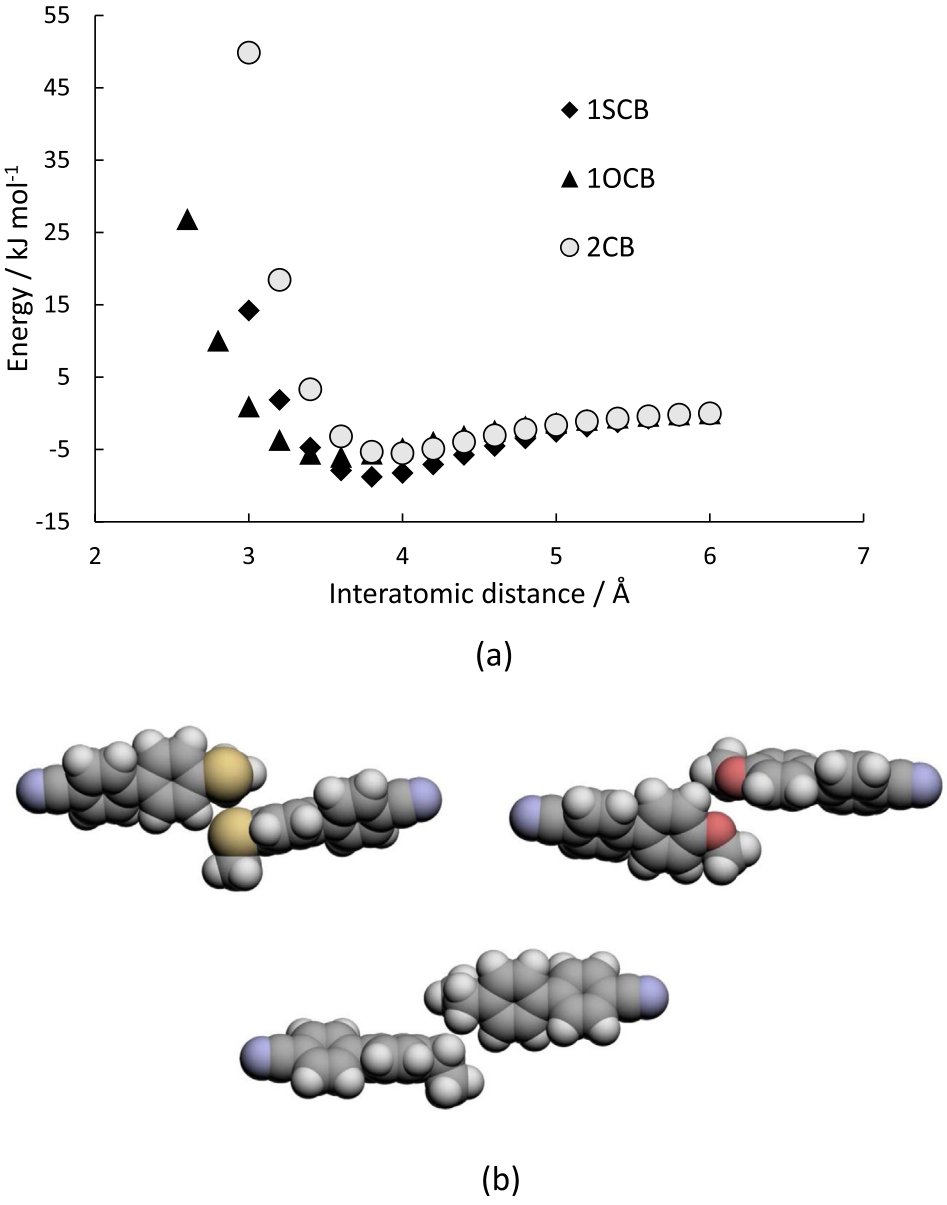

Fig. 7. (a) The dependence of the total (BSSE corrected) energy of each pair of molecules (1SCB, 1OCB and 2CB). For each compound, the energy calculated at 6 Å separation is defined as 0 kJ mol^{-1}. (b) The molecular pairs corresponding to the calculated energy minima.

These steric and electronic considerations weaken the chalcogen bond, and T_{NI} falls sharply between 1SCB and 3SCB. The similarity in behaviour between the nSCB and nCB series for longer chains supports the view that the chalcogen bonding is no longer as significant. There are insufficient data available, however, to comment generally on the effect on the clearing temperature of exchanging an alkyl for alkylthio chain of the same overall length. It would be expected that the enhanced flexibility and smaller C-S-C bond angle for the alkylthio chain would serve to decrease the clearing temperature (Fig. 4). Countering this reduction is the enhanced anisotropic polarizability arising from the introduction of the sulfur atom which would be expected to increase the interactions between the mesogenic cores and increase the clearing temperature. Indeed substituting sulfur for oxygen in chalcogeno esters resulted in an increase in the clearing temperature, and this was attributed to the associated increase in the anisotropic polarizability [40]. The similarity in the clearing temperatures of the nSCB and nCB series for longer chain lengths suggests that these opposing contributions are more or less balanced. This view is consistent with the observation that the lateral separation in nematic phases formed by alkylthio-containing materials is slightly smaller than that between the analogous alkyloxy-substituted materials [20,41] and that alkylthio-containing materials have a strong ten-dency to exhibit cybotactic behaviour in the nematic phase [19,20,41,42]. Both observations suggest stronger interactions between the mesogenic units. It has also been suggested that the strong temperature dependence of the birefringence measured for alkylthio-containing nematogens may be attributed, at least in part, to sulfur-sulfur interactions [21,43].

4. Conclusions

Our understanding of chalcogen-bonding interactions and their role in determining liquid crystalline behaviour is at an embryonic stage. Much work needs to be done to establish the steric and electronic factors that influence this newest of tools in the design of liquid crystals having tailored properties with application potential in a range of diverse areas. The challenge is to establish whether chalcogen bonding can be used in the design of new mesogenic materials in a similar fashion to hydrogen bonding and halogen bonding, and extend the chemist's toolbox in the search for new materials. In the case of hydrogen and halogen bonding, these interactions are used to assemble what may be considered to be the mesogenic core of a supramolecular complex and which exists in a dynamic equilibrium with the donor and acceptor [44,45]. It appears more likely that, given the relative strength and geometric constraints of the chalcogen bond, the emerging role of chalcogen bonding will be to modify existing liquid crystalline behaviour rather than to induce it in mixtures of non-mesogenic components.

Declaration of Competing Interest

The authors declare that they have no known competing financial interests or personal relationships that could have appeared to influence the work reported in this paper.

Acknowledgement

This research did not receive any specific grant from funding agencies in the public, commercial, or not-for-profit sectors.

References

[1] T. Kato, J.M.J. Frechet, New approach to mesophase stabilization through hydrogen-bonding molecular-interactions in binary-mixtures 8533 J Am Chem Soc. 111 (1989).
[2] R. Walker, D. Pociecha, A. Martinez-Felipe, J.MD. Storey, E. Gorecka, C.T. Imrie, Twist-Bend Nematogenic Supramolecular Dimers and Trimers Formed by Hydrogen Bonding, Crystals. 10 (3) (2020) 175, https://doi.org/10.3390/cryst10030175.
[3] R. Walker, D. Pociecha, C.A. Crawford, J.M.D. Storey, E. Gorecka, C.T. Imrie, Hydrogen bonding and the design of twist-bend nematogens, J Molec Liq. 303 (2020) 112630, https://doi.org/10.1016/j.molliq.2020.112630.
[4] J. Knelles, C. Wanner, F. Schulz, M. Freund, M.A. Kolmangadi, A. Baro, P. Huber, A. Schonhals, S. Laschat, Liquid crystalline hydrazones revisited: dipolar interactions vs hydrogen bonding affecting mesomorphic properties, Liq Cryst. (2021), https://doi.org/10.1080/02678292.2021.1873438.
[5] S.S. Nafee, H.A. Ahmed, M. Hagar, New architectures of supramolecular H-bonded liquid crystal complexes based on dipyridine derivatives, Liq Crys. 47 (12) (2020) 1811–1824.
[6] M. Fouzai, A. Guesmi, N.B. Hamadi, T. Soltani, Fluoro-substitution in hydrogen bonding liquid crystal benzoic acid: dielectric, electro-optic and optical proprieties and inducing polar nematic phase, Liq Cryst. 47 (5) (2020) 777–784.
[7] H.L. Nguyen, P.N. Horton, M.B. Hursthouse, A.C. Legon, D.W. Bruce, Halogen bonding: A new interaction for liquid crystal formation 16 J Am Chem Soc. 126 (2004).
[8] C. Wespiser, J. Xu, A. Soldera, Atomistic simulation of the smectic a mesophase induced by halogen bond, J Molec Liq. 319 (2020) 113731, https://doi.org/ 10.1016/j.molliq.2020.113731.
[9] L. Barcelona-Cazanave, N. Trejo-Carbajal, R.J. Rodríguez-González, L. Larios-López, I. Felix-Serrano, J.M. Mata-Padilla, D. Navarro-Rodríguez, Synthesis and thermotropic liquid-crystalline properties of a hexyloxy-substituted pyridyl-ethynylene-azobenzene and its halogen-bonded complex with tetrafluoroiodophenyl decanoate, J Fluorine Chem. 244 (2021) 109739, https://doi.org/10.1016/j.jfluchem.2021.109739.
[10] D. Devadiga, T.N. Ahipa, An up-to-date review on halogen-bonded liquid crystals, J Molec Liq. 333 (2021) 115961, https://doi.org/10.1016/j.molliq.2021.115961.
[11] S. Nath, A. Kappelt, M. Spengler, B. Roy, J. Voskuhl, M. Giese, Tuning the solid-state emission of liquid crystalline nitro-by halogen bonding 124 Beilstein J Org Chem. 17 (2021).
[12] Y. Huang, X. Zhang, W. Cui, X. Wang, B. Li, Y. Zhang, J. Yang, Novel liquid crystalline organogelators based on terephthalic acid and terephthalaldehyde derivatives: properties and promotion through the formation of halogen bonding, New J Chem. 44 (2) (2020) 614–625.
[13] L. Vogel, P. Wonner, S.M. Huber, Chalcogen Bonding: An Overview, Angew Chem Int Ed. 58 (7) (2019) 1880–1891.
[14] I.S. Antonijević, G.V. Janjić, M.K. Milčić, S.D. Zarić, Preferred Geometries and Energies of Sulfur Sulfur Interactions in Crystal Structures, Crys Growth Design. 16 (2) (2016) 632–639.
[15] N. Biot, D. Bonifazi, Chalcogen-bond driven molecular recognition at work, Coord Chem Rev. 413 (2020) 213243, https://doi.org/10.1016/j. ccr.2020.213243.
[16] P.C. Ho, J.Z. Wang, F. Meloni, I. Vargas-Baca, Chalcogen bonding in materials chemistry, Coord Chem Rev. 422 (2020) 213464, https://doi.org/10.1016/j. ccr.2020.213464.
[17] P. Scilabra, G. Terraneo, G. Resnati, The Chalcogen Bond in Crystalline Solids: A World Parallel to Halogen Bond, Acc Chem Res. 52 (5) (2019) 1313–1324.
[18] K.T. Mahmudov, M.N. Kopylovich, M.F.C. Guedes da Silva, A.J.L. Pombeiro, Chalcogen bonding in synthesis, catalysis and design of materials, Dalton Trans. 46 (31) (2017) 10121–10138.
[19] Y. Arakawa, S. Inui, K. Igawa, H. Tsuji, Alkylthio- and alkyl-substituted asymmetric diphenyldiacetylene-based liquid crystals: phase transitions, mesophase and single-crystal structures, and birefringence, Liq Cryst. 46 (11) (2019) 1621–1630.
[20] Y. Arakawa, Y. Sasaki, N. Haraguchi, S. Itsuno, H. Tsuji, Synthesis, phase transitions and birefringence of novel liquid crystalline 1,4-phenylene bis(4-alkylthio benzoates) and insights into the cybotactic nematic behaviour, Liq Cryst. 45 (6) (2018) 821–830.
[21] Y. Arakawa, S. Kang, H. Tsuji, J. Watanabe, G.-I. Konishi, Development of novel bistolane-based liquid crystalline molecules with an alkylsulfanyl group for highly birefringent materials, RSC Adv. 6 (20) (2016) 16568–16574.
[22] J. Herman, P. Kula, Design of new super-high birefringent isothiocyanato bistolanes - synthesis and properties, Liq Cryst. 44 (9) (2017) 1462–1467.
[23] Y. Arakawa, H. Tsuji, Phase transitions and birefringence of bistolane-based nematic molecules with an alkyl, alkoxy and alkylthio group, Molec Cryst Liq Cryst. 647 (1) (2017) 422–429.
[24] Y. Arakawa, Y. Ishida, H. Tsuji, Etherand Thioether-Linked Naphthalene-Based Liquid-Crystal Dimers: Influence of Chalcogen Linkage and Mesogenic-Arm Symmetry on the Incidence and Stability of the Twist-Bend Nematic Phase, Chem Eur J. 26 (17) (2020) 3767–3775.
[25] Y. Arakawa, K. Komatsu, H. Tsuji, Twist-bend nematic liquid crystals based on thioether linkage, New J Chem. 43 (17) (2019) 6786–6793.
[26] E. Cruickshank, M. Salamoń czyk, D. Pociecha, G.J. Strachan, J.M.D. Storey, C. Wang, J. Feng, C. Zhu, E. Gorecka, C.T. Imrie, Sulfur-linked cyanobiphenyl-based liquid crystal dimers and the twist-bend nematic phase, Liq Cryst. 46 (10) (2019) 1595–1609.
[27] H.-C. Lee, Z. Lu, P.A. Henderson, M.F. Achard, W.A.K. Mahmood, G.-Y. Yeap, C.T. Imrie, Cholesteryl-based liquid crystal dimers containing a sulfur-sulfur link in the flexible spacer, Liq Cryst. 39 (2) (2012) 259–268.
[28] G.W. Gray, K.J. Harrison, J.A. Nash, New family of nematic liquid-crystals for displays, Electronics Lett. 9 (6) (1973) 130, https://doi.org/10.1049/el:19730096.
[29] M.J. Frisch et al., Gaussian 09 (Revision B.01), Gaussian Inc., Wallingford CT, 2010.
[30] M. Tarini, P. Cignoni, C. Montani, Ambient Occlusion and Edge Cueing for Enhancing Real Time Molecular Visualization IEEE Trans Visualization and Computer Graphics. 12 (5) (2006) 1237–1244.
[31] A.J. Seed, K.J. Toyne, J.W. Goodby, Synthesis of the series of monofluoro-substituted 4-butylsulfanyl-4'-cyanobiphenyls and effect of the position of fluorine within the core on refractive indices, optical anisotropies, polarisabilities and order parameters, J Mater Chem. 5 (12) (1995) 2201–2207.
[32] G.A. Oweimreen, M.A. Morsy, DSC studies on p-(n-alkyl)-p '-cyanobiphenyl (RCB's) and p-(n-alkoxy)-p '-cyanobiphenyl (ROCB's) liquid crystals, Thermochim Acta. 346 (1-2) (2000) 37–47.
[33] D.A. Paterson, C.A. Crawford, D. Pociecha, R. Walker, J.M.D. Storey, E. Gorecka, C.T. Imrie, The role of a terminal chain in promoting the twist-bend nematic phase: the synthesis and characterisation of the 1-(4-cyanobiphenyl-4 '-yl)-6-(4-alkyloxyanilinebenzylidene-4 '-oxy)hexanes, Liq Cryst. 45 (13-15) (2018) 2341–2351.
[34] R. Walker, D. Pociecha, G.J. Strachan, J.M.D. Storey, E. Gorecka, C.T. Imrie, Molecular curvature, specific intermolecular interactions and the twist-bend nematic phase: the synthesis and characterisation of the 1-(4-cyanobiphenylyl)-6-(4-alkylanilinebenzylidene-4-oxy)hexanes (CB6O.m), Soft Matter 15 (15) (2019) 3188–3197.

[35] J.W. Emsley, G. De Luca, G. Celebre, M. Longeri, The conformation of the aromatic rings relative to the alkyl chain in 4-n-pentyl-4'-cyanobiphenyl, Liq Cryst. 20 (5) (1996) 569-575.

[36] D.A. Paterson, M. Gao, Y.-K. Kim, A. Jamali, K.L. Finley, B. Robles-Hernández, S. Diez-Berart, J. Salud, M.R. de la Fuente, B.A. Timimi, H. Zimmermann, C. Greco, A. Ferrarini, J.M.D. Storey, D.O. López, O.D. Lavrentovich, G.R. Luckhurst, C.T. Imrie, Understanding the twist-bend nematic phase: the characterisation of 1-(4-cyanobiphenyl-4 '-yloxy)-6-(4-cyanobiphenyl-4 '-yl)hexane (CB6OCB) and comparison with CB7CB, Soft Matter 12 (32) (2016) 6827–6840.

[37] Y.L. Frolov, A.V. Vashchenko, Quantum-chemical study of methyl phenyl sulfide, Russian J Org Chem. 39 (10) (2003) 1412–1414.

[38] Y. Arakawa, S. Inui, H. Tsuji, Novel diphenylacetylene-based room-temperature liquid crystalline molecules with alkylthio groups, and investigation of the role for terminal alkyl chains in mesogenic incidence and tendency, Liq Cryst. 45 (6) (2018) 811–820.

[39] Y. Arakawa, Y. Sasaki, H. Tsuji, Supramolecular hydrogen-bonded liquid crystals based on 4-n-alkylthiobenzoic acids and 4,4 '-bipyridine: Their mesomorphic behavior with comparative study including alkyl and alkoxy counterparts, J Molec Liq. 280 (2019) 153–159.

[40] D.S. Rampon, F.S. Rodembusch, P.F.B. Gonçalves, R.V. Lourega, A.A. Merlo, P.H. Schneider, An Evaluation of the Chalcogen Atom Effect on the Mesomorphic and Electronic Properties in a New Homologous Series of Chalcogeno Esters, J Brazilian Chem Soc. 21 (11) (2010) 2100–2107.

[41] Y. Arakawa, S. Kang, J. Watanabe, G.-I. Konishi, Assembly of thioether-containing rod-like liquid crystalline materials assisted by hydrogen-bonding terminal carboxyl groups, RSC Adv. 5 (11) (2015) 8056–8062.

[42] Y. Arakawa, Y. Sasaki, H. Tsuji, Novel Hydrogen-bonded Liquid Crystalline Complexes between 4-Alkylthiobenzoic Acids and 4-Phenylpyridine, Chem Lett. 46 (11) (2017) 1657–1659.

[43] Y. Arakawa, S. Kang, H. Tsuji, J. Watanabe, G.-I. Konishi, The design of liquid crystalline bistolane-based materials with extremely high birefringence, RSC Adv. 6 (95) (2016) 92845–92851.

[44] A. Martinez-Felipe, A.G. Cook, J.P. Abberley, R. Walker, J.M.D. Storey, C.T. Imrie, An FT-IR spectroscopic study of the role of hydrogen bonding in the formation of liquid crystallinity for mixtures containing bipyridines and 4-pentoxybenzoic acid, RSC Adv. 6 (110) (2016) 108164–108179.

[45] A. Martínez-Felipe, A.G. Cook, M.J. Wallage, C.T. Imrie, Hydrogen bonding and liquid crystallinity of low molar mass and polymeric mesogens containing benzoic acids: a variable temperature Fourier transform infrared spectroscopic study, Phase Trans. 87 (12) (2014) 1191–1210.

Supplementary Information

Chalcogen bonding and liquid crystallinity: understanding the anomalous behaviour of the 4'-(alkylthio)[1,1'-biphenyl]-4-carbonitriles (nSCB)

Ewan Cruickshank, Grant J Strachan, John MD Storey, and Corrie T Imrie*

Department of Chemistry, School of Natural and Computing Sciences, University of Aberdeen, Meston Building, Aberdeen AB24 3UE, UK

*Author for correspondence; email c.t.imrie@abdn.ac.uk

1.0 General Information

1.0.1 Reagents

All reagents and solvents that were available commercially were purchased from Sigma Aldrich, Fisher Scientific or Fluorochem and were used without further purification unless otherwise stated.

1.0.2 Thin Layer Chromatography

Reactions were monitored using thin layer chromatography, and the appropriate solvent system, using aluminium-backed plates with a coating of Merck Kieselgel 60 F254 silica which were purchased from Merck KGaA. The spots on the plate were visualised by UV light (254 nm) or by oxidation using either a potassium permanganate stain or iodine dip.

1.0.3 Column Chromatography

For normal phase column chromatography, the separations were carried out using silica gel grade 60 Å, 40-63 μm particle size, purchased from Fluorochem and using an appropriate solvent system.

1.0.4 Structure Characterisation

All final products and intermediates that were synthesised were characterised using ^{1}H NMR, ^{13}C NMR and infrared spectroscopies. The ^{1}H and ^{13}C NMR spectra were recorded on either a 400 MHz Bruker Avance III HD NMR spectrometer, or a 300 MHz Bruker Ultrashield NMR spectrometer. The infrared spectra were recorded on a Thermal Scientific Nicolet IR100 FTIR spectrometer with an ATR diamond cell.

1.0.5 Purity Analysis

In order to determine the purity of the final products, elemental analysis was used. C, H, N, S microanalysis were carried out by the Elemental Analysis Service at OEA Laboratories Limited using a CE Instruments EA1110 CHNS-O Elemental Analyser. The instrument was calibrated using series of different weights of sulphanilamide and acetanilide.

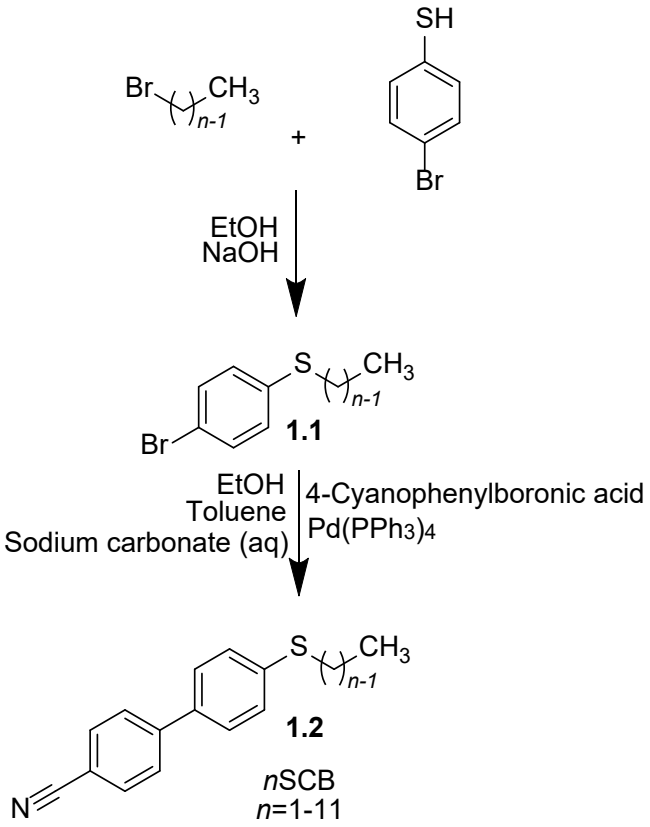

Scheme 1.1. Synthesis of *n*SCB.

1.1 1-Bromo-4-(alkylthio)benzenes

To a pre-dried flask flushed with argon, 4-bromothiophenol (1.1 eq, 1.00 g, 5.29×10^{-3} mol) was added. Sodium hydroxide (1.32 eq, 0.254 g, $6.35\text{x}10^{-3}$ mol) in ethanol (40 mL), sonicated to ensure all the solid was in solution, was added and the reaction mixture was stirred for 2 h at room temperature. The appropriate 1-bromoalkane (1.0 eq) was added to the flask and the reaction mixture was stirred at room temperature for 24 h. The quantities of 1-bromoalkane used in each reaction are listed in **Table 1.1**. During the course of the reaction a white precipitate, sodium bromide, formed. The extent of the reaction was monitored by TLC using 30 % 40:60 petroleum ether and 70 % dichloromethane as the solvent system (RF values quoted in the product data). At the end of the reaction the sodium bromide solid was removed using vacuum filtration and collected solvent was evaporated under vacuum to leave the desired product as either a colourless oil or a white solid, which was used without further purification.

Table 1.1. Quantities of 1-bromoalkane used in the syntheses of 1-bromo-4-(alkylthio)benzenes (**1.1**).

n	1-Bromoalkane
2	0.36 mL, 0.524 g, 4.81×10^{-3} mol
3	0.44 mL, 0.592 g, 4.81×10^{-3} mol
4	0.52 mL, 0.659 g, 4.81×10^{-3} mol
5	0.60 mL, 0.727 g, 4.81×10^{-3} mol
6	0.68 mL, 0.794 g, 4.81×10^{-3} mol
7	0.76 mL, 0.861 g, 4.81×10^{-3} mol
8	0.83 mL, 0.928 g, 4.81×10^{-3} mol
9	0.92 mL, 1.00 g, 4.81×10^{-3} mol
10	1.00 mL, 1.06 g, 4.81×10^{-3} mol
11	1.07 mL, 1.13 g, 4.81×10^{-3} mol

1-Bromo-4-(methylthio)benzene - Was purchased commercially from Sigma Aldrich and used without further purification.

1.1.1 1-Bromo-4-(ethylthio)benzene

Colourless oil. Yield: 0.893 g, 85.5 %. RF: 0.76

ν_{max}/cm^{-1}: 2972, 2926, 2869, 1472, 1447, 1386, 1264, 1091, 1069, 1005, 805, 763, 728, 508, 478

δ_H/ppm (400 MHz, $CDCl_3$): 7.39 (2 H, d, J 7.8 Hz, Ar-H), 7.18 (2 H, d, J 7.8 Hz, Ar-H), 2.92 (2 H, quart, J 7.4 Hz, S-$\underline{CH_2}$-CH_3), 1.30 (3 H, t, J 7.4 Hz, S-CH_2-$\underline{CH_3}$)

δ_C/ppm (100 MHz, $CDCl_3$): 135.90, 131.85, 130.49, 119.51, 27.73, 14.25

Data consistent with reported values [1]

1.1.2 1-Bromo-4-(propylthio)benzene

Colourless oil. Yield: 1.00 g, 89.9 %. RF: 0.74

ν_{max}/cm^{-1}: 2961, 2929, 2871, 1472, 1386, 1290, 1237, 1091, 1069, 1006, 804, 728, 507, 479

δ_H/ppm (400 MHz, $CDCl_3$): 7.39 (2 H, d, J 7.9 Hz, Ar-H), 7.18 (2 H, d, J 7.9 Hz, Ar-H), 2.88 (2 H, t, J 7.3 Hz, S-$\underline{CH_2}$-CH_2-), 1.66 (2 H, sext, J 7.3 Hz, S-CH_2-$\underline{CH_2}$-CH_3), 1.02 (3 H, t, J 7.3 Hz, S-CH_2-CH_2-$\underline{CH_3}$)

δ_C/ppm (100 MHz, $CDCl_3$): 136.22, 131.83, 130.45, 119.40, 35.68, 22.40, 13.41

Data consistent with reported values [1]

1.1.3 1-Bromo-4-(butylthio)benzene

Colourless oil. Yield: 1.09 g, 92.4 %. RF: 0.74

ν_{max}/cm^{-1}: 2956, 2928, 2871, 1472, 1436, 1385, 1091, 1069, 1006, 804, 728, 508, 479

δ_H/ppm (400 MHz, $CDCl_3$): 7.39 (2 H, d, J 7.7 Hz, Ar-H), 7.17 (2 H, d, J 7.7 Hz, Ar-H), 2.89 (2 H, t, J 7.4 Hz, S-$\underline{CH_2}$-CH_2-), 1.62 (2 H, quin, J 7.4 Hz, S-CH_2-$\underline{CH_2}$-CH_2-), 1.44 (2 H, sext, J 7.4 Hz, S-CH_2-CH_2-$\underline{CH_2}$-CH_3), 0.92 (3 H, t, J 7.4 Hz, S-CH_2-CH_2-CH_2-$\underline{CH_3}$)

δ_C/ppm (100 MHz, $CDCl_3$): 136.32, 131.83, 130.33, 119.35, 33.35, 31.08, 21.94, 13.64

Data consistent with reported values [2]

1.1.4 1-Bromo-4-(pentylthio)benzene

Colourless oil. Yield: 1.20 g, 96.2 %. RF: 0.74

ν_{max}/cm^{-1}: 2954, 2927, 2857, 1473, 1385, 1092, 1069, 1006, 804, 728, 509, 479

δ_H/ppm (400 MHz, $CDCl_3$): 7.39 (2 H, d, J 7.9 Hz, Ar-H), 7.17 (2 H, d, J 7.9 Hz, Ar-H), 2.88 (2 H, t, J 7.4 Hz, S-$\underline{CH_2}$-CH_2-), 1.63 (2 H, quin, J 7.4 Hz, S-CH_2-$\underline{CH_2}$-CH_2-), 1.36 (4 H, m, S-CH_2-CH_2-$\underline{CH_2}$-$\underline{CH_2}$-CH_3), 0.90 (3 H, t, J 6.7 Hz, S-CH_2-CH_2-CH_2-CH_2-$\underline{CH_3}$)

δ_C/ppm (100 MHz, $CDCl_3$): 136.34, 131.82, 130.30, 119.34, 33.63, 30.98, 28.70, 22.25, 13.98

1.1.5 1-Bromo-4-(hexylthio)benzene

Colourless oil. Yield: 0.341 g, 25.9 %. RF: 0.74

ν_{max}/cm^{-1}: 2954, 2926, 2855, 1473, 1385, 1092, 1069, 1006, 804, 727, 479

δ_H/ppm (400 MHz, $CDCl_3$): 7.38 (2 H, d, J 7.9 Hz, Ar-H), 7.17 (2 H, d, J 7.9 Hz, Ar-H), 2.88 (2 H, t, J 7.5 Hz, S-$\underline{CH_2}$-CH_2-), 1.63 (2 H, quin, J 7.5 Hz, S-CH_2-$\underline{CH_2}$-CH_2-), 1.41 (2 H, quin, J 7.5 Hz, S-CH_2-CH_2-$\underline{CH_2}$-CH_2-), 1.27 (4 H, m, S-CH_2-CH_2-CH_2-$\underline{CH_2}$-$\underline{CH_2}$-CH_3), 0.89 (3 H, t, J 7.0 Hz, S-CH_2-CH_2-CH_2-CH_2-CH_2-$\underline{CH_3}$)

δ_C/ppm (100 MHz, $CDCl_3$): 136.33, 131.82, 130.32, 119.34, 33.67, 31.35, 28.98, 28.49, 22.54, 14.03

1.1.6 1-Bromo-4-(heptylthio)benzene

Colourless oil. Yield: 1.14 g, 82.5 %. RF: 0.74

ν_{max}/cm^{-1}: 2953, 2924, 2853, 1473, 1386, 1092, 1069, 1006, 804, 727, 479

δ_H/ppm (400 MHz, $CDCl_3$): 7.38 (2 H, d, J 7.9 Hz, Ar-H), 7.17 (2 H, d, J 7.9 Hz, Ar-H), 2.89 (2 H, t, J 7.4 Hz, S-$\underline{CH_2}$-CH_2-), 1.63 (2 H, quin, J 7.4 Hz, S-CH_2-$\underline{CH_2}$-CH_2-), 1.41 (2 H, quin,

J 7.4 Hz, S-CH_2-CH_2-$\underline{CH_2}$-CH_2-), 1.29 (6 H, m, S-CH_2-CH_2-CH_2-$\underline{CH_2}$-$\underline{CH_2}$-$\underline{CH_2}$-CH_3), 0.88 (3 H, t, J 6.7 Hz, S-CH_2-CH_2-CH_2-CH_2-CH_2-CH_2-$\underline{CH_3}$)

δ_C/ppm (100 MHz, $CDCl_3$): 136.34, 131.82, 130.32, 119.34, 33.67, 31.70, 29.01, 28.83, 28.77, 22.60, 14.09

1.1.7 1-Bromo-4-(octylthio)benzene

White solid. Yield: 1.26 g, 86.9 %. RF: 0.74. MP: 26 °C

ν_{max}/cm^{-1}: 2950, 2922, 2849, 1470, 1425, 1386, 1282, 1094, 1069, 1006, 803, 753, 722, 515, 479

δ_H/ppm (400 MHz, $CDCl_3$): 7.38 (2 H, d, J 7.7 Hz, Ar-H), 7.17 (2 H, d, J 7.7 Hz, Ar-H), 2.89 (2 H, t, J 7.4 Hz, S-$\underline{CH_2}$-CH_2-), 1.63 (2 H, quin, J 7.4 Hz, S-CH_2-$\underline{CH_2}$-CH_2-), 1.41 (2 H, quin, J 7.4 Hz, S-CH_2-CH_2-$\underline{CH_2}$-CH_2-), 1.27 (8 H, m, S-CH_2-CH_2-CH_2-$\underline{CH_2}$-$\underline{CH_2}$-$\underline{CH_2}$-$\underline{CH_2}$-CH_3), 0.88 (3 H, t, J 6.9 Hz, S-CH_2-CH_2-CH_2-CH_2-CH_2-CH_2-CH_2-$\underline{CH_3}$)

δ_C/ppm (100 MHz, $CDCl_3$): 136.34, 131.82, 130.32, 119.34, 33.67, 31.80, 29.17, 29.12, 29.01, 28.81, 22.66, 14.11

1.1.8 1-Bromo-4-(nonylthio)benzene

White solid. Yield: 1.31 g, 86.4 %. RF: 0.74. MP: 31 °C

ν_{max}/cm^{-1}: 2951, 2917, 2849, 1473, 1463, 1385, 1264, 1091, 1073, 1005, 805, 728, 719, 512, 485, 474

δ_H/ppm (400 MHz, $CDCl_3$): 7.38 (2 H, d, J 7.8 Hz, Ar-H), 7.17 (2 H, d, J 7.8 Hz, Ar-H), 2.88 (2 H, t, J 7.5 Hz, S-$\underline{CH_2}$-CH_2-), 1.62 (2 H, quin, J 7.5 Hz, S-CH_2-$\underline{CH_2}$-CH_2-), 1.40 (2 H, quin, J 7.5, S-CH_2-CH_2-$\underline{CH_2}$-CH_2-), 1.27 (10 H, m, S-CH_2-CH_2-CH_2-$\underline{CH_2}$-$\underline{CH_2}$-$\underline{CH_2}$-$\underline{CH_2}$-$\underline{CH_2}$-CH_3), 0.88 (3 H, t, J 6.8 Hz, S-CH_2-CH_2-CH_2-CH_2-CH_2-CH_2-CH_2-CH_2-$\underline{CH_3}$)

δ_C/ppm (100 MHz, $CDCl_3$): 136.33, 131.82, 130.33, 119.34, 33.67, 31.86, 29.45, 29.24, 29.15, 29.01, 28.80, 22.68, 14.12

1.1.9 1-Bromo-4-(decylthio)benzene

White solid. Yield: 1.39 g, 87.7 %. RF: 0.72. MP: 37 °C

ν_{max}/cm^{-1}: 2950, 2916, 2846, 1467, 1384, 1093, 1068, 1005, 803, 721, 514, 480, 475

δ_H/ppm (400 MHz, $CDCl_3$): 7.38 (2 H, d, J 8.1 Hz, Ar-H), 7.17 (2 H, d, J 8.1 Hz, Ar-H), 2.88 (2 H, t, J 7.4 Hz, S-$\underline{CH_2}$-CH_2-), 1.63 (2 H, quin, J 7.4 Hz, S-CH_2-$\underline{CH_2}$-CH_2-), 1.40 (2 H, quin, J 7.4 Hz, S-CH_2-CH_2-$\underline{CH_2}$-CH_2-), 1.26 (12 H, m, S-CH_2-CH_2-CH_2-$\underline{CH_2}$-$\underline{CH_2}$-$\underline{CH_2}$-$\underline{CH_2}$-$\underline{CH_2}$-$\underline{CH_2}$-CH_3), 0.88 (3 H, t, J 7.0 Hz, S-CH_2-CH_2-CH_2-CH_2-CH_2-CH_2-CH_2-CH_2-CH_2-$\underline{CH_3}$)

δ_C/ppm (100 MHz, $CDCl_3$): 136.32, 131.82, 130.32, 119.33, 33.67, 31.89, 29.53, 29.49, 29.31, 29.15, 29.00, 28.80, 22.69, 14.13

1.1.10 1-Bromo-4-(undecylthio)benzene

White solid. Yield: 1.55 g, 93.8 %. RF: 0.72. MP: 41 °C

ν_{max}/cm^{-1}: 2951, 2916, 2848, 1472, 1462, 1385, 1091, 1074, 1005, 806, 728, 718, 515, 485, 474

δ_H/ppm (400 MHz, $CDCl_3$): 7.38 (2 H, d, J 8.1 Hz, Ar-H), 7.17 (2 H, d, J 8.1 Hz, Ar-H), 2.88 (2 H, t, J 7.4 Hz, S-$\underline{CH_2}$-CH_2-), 1.62 (2 H, quin, J 7.4 Hz, S-CH_2-$\underline{CH_2}$-CH_2-), 1.40 (2 H, quin, J 7.4 Hz, S-CH_2-CH_2-$\underline{CH_2}$-CH_2-), 1.26 (14 H, m, S-CH_2-CH_2-CH_2-$\underline{CH_2}$-$\underline{CH_2}$-$\underline{CH_2}$-$\underline{CH_2}$-$\underline{CH_2}$-$\underline{CH_2}$-CH_3), 0.88 (3 H, t, J 7.0 Hz, S-CH_2-CH_2-CH_2-CH_2-CH_2-CH_2-CH_2-CH_2-CH_2-$\underline{CH_3}$)

δ_C/ppm (100 MHz, $CDCl_3$): 136.33, 131.82, 130.32, 119.33, 33.67, 31.91, 29.60, 29.58, 29.49, 29.34, 29.15, 29.00, 28.80, 22.70, 14.13

1.2 4'-(Alkylthio)[1,1'-biphenyl]-4-carbonitriles (*n*SCB)

To a pre-dried flask fitted with a condenser and flushed with argon, compound **1.1** (1 eq), 4-cyanophenylboronic acid (1.1 eq) and tetrakis(triphenylphosphine)palladium(0) (0.025 eq) were added. A mixture of aqueous sodium carbonate (2 M, 10 mL), ethanol (5 mL) and toluene (40 mL) was added, and the reaction mixture was heated to 85 °C for 24 hours with stirring. The quantities of the reagents used in each reaction are listed in **Table 1.2**. The reaction mixture was cooled to room temperature and 32 % hydrochloric acid (5 mL) was added dropwise until effervescence was no longer observed. The resulting mixture was filtered using vacuum filtration to remove the palladium catalyst, and the solvents removed under vacuum. Water (100 mL) and dichloromethane (100 mL) were added to the solid obtained. The organic layer was washed with water (2 × 50 mL) and dried over anhydrous magnesium sulphate. The magnesium sulphate was removed by vacuum filtration and the solvent removed under vacuum to give a brown/tan solid. The crude product was purified using a silica gel column with 30 % 40:60 petroleum ether and 70 % dichloromethane as eluent (RF values quoted in product data). The eluent fractions of interest were evaporated under vacuum to leave a white solid which was recrystallised from hot ethanol (20 mL). Due to slight solubility with ethanol, the flask for recrystallisation was placed in ice prior to vacuum filtration.

Table 1.2. Quantities of reagents used in the syntheses of the 4'-(alkylthio)-[1,1'-biphenyl]-4-carbonitriles (**1.2**).

n	(**1.1**)	4-Cyanophenylboronic acid	Tetrakis(triphenylphosphine) palladium(0)
1	0.80 g, 3.94×10^{-3} mol	0.636 g, 4.33×10^{-3} mol	0.114 g, 9.85×10^{-5} mol
2	0.75 g, 3.47×10^{-3} mol	0.561 g, 3.82×10^{-3} mol	0.100 g, 8.68×10^{-5} mol
3	0.80 g, 3.48×10^{-3} mol	0.558 g, 3.80×10^{-3} mol	0.100 g, 8.65×10^{-5} mol
4	0.85 g, 3.47×10^{-3} mol	0.561 g, 3.82×10^{-3} mol	0.100 g, 8.68×10^{-5} mol
5	1.10 g, 4.24×10^{-3} mol	0.686 g, 4.67×10^{-3} mol	0.122 g, 1.06×10^{-4} mol
6	0.30 g, 1.10×10^{-3} mol	0.178 g, 1.21×10^{-3} mol	0.064 g, 5.50×10^{-5} mol
7	0.95 g, 3.31×10^{-3} mol	0.535 g, 3.64×10^{-3} mol	0.096 g, 8.30×10^{-5} mol
8	1.00 g, 3.32×10^{-3} mol	0.536 g, 3.65×10^{-3} mol	0.096 g, 8.30×10^{-5} mol
9	1.10 g, 3.49×10^{-3} mol	0.564 g, 3.84×10^{-3} mol	0.101 g, 8.73×10^{-5} mol
10	1.20 g, 3.64×10^{-3} mol	0.589 g, 4.01×10^{-3} mol	0.105 g, 9.10×10^{-5} mol
11	1.40 g, 4.08×10^{-3} mol	0.658 g, 4.48×10^{-3} mol	0.118 g, 1.02×10^{-4} mol

1.2.1 4'-(Methylthio)-[1,1'-biphenyl]-4-carbonitrile (1SCB)

Yield: 0.496 g, 55.8 %. RF: 0.38

T_{Cr-} 135 °C T_{NI} (78 °C)

ν_{max}/cm^{-1}: 2222, 1603, 1594, 1484, 1439, 1391, 1094, 850, 810, 733, 562, 522

δ_H/ppm (400 MHz, $CDCl_3$): 7.71 (2 H, d, J 8.1 Hz, Ar-H), 7.66 (2 H, d, J 8.1 Hz, Ar-H), 7.52 (2 H, d, J 7.9 Hz, Ar-H), 7.40 (2 H, d, J 7.9 Hz, Ar-H), 2.53 (3 H, s, S-$\underline{CH_3}$)

δ_C/ppm (100 MHz, $CDCl_3$): 144.97, 139.86, 135.60, 132.65, 127.48, 127.30, 126.71, 118.96, 110.71, 15.52

Elemental Analysis: Calculated for $C_{14}H_{11}NS$: C = 74.63 %, H = 4.92 %, N = 6.45 %, S = 14.23 %; Found: C = 75.00 %, H = 5.01 %, N = 6.26 %, S = 14.25 %

1.2.2 4'-(Ethylthio)-[1,1'-biphenyl]-4-carbonitrile (2SCB)

Yield: 0.276 g, 33.2 %. RF: 0.42

T_{Cr-} 82 °C T_{NI} (53 °C)

ν_{max}/cm^{-1}: 2931, 2227, 1605, 1589, 1484, 1454, 1436, 1394, 1258, 1183, 1094, 998, 851, 811, 766, 558, 520

δ_H/ppm (400 MHz, $CDCl_3$): 7.71 (2 H, d, J 7.9 Hz, Ar-H), 7.66 (2 H, d, J 7.9 Hz, Ar-H), 7.51 (2 H, d, J 7.7 Hz, Ar-H), 7.40 (2 H, d, J 7.7 Hz, Ar-H), 3.01 (2 H, quart, J 7.3 Hz, S-$\underline{CH_2}$-CH_3), 1.37 (3 H, t, J 7.3 Hz, S-CH_2-$\underline{CH_3}$)

δ_C/ppm (100 MHz, $CDCl_3$): 144.95, 138.22, 136.19, 132.65, 128.72, 127.52, 127.35, 118.94, 110.79, 27.14, 14.26

Elemental Analysis: Calculated for $C_{15}H_{13}NS$: C = 75.28 %, H = 5.48 %, N = 5.85 %, S = 13.40 %; Found: C = 75.43 %, H = 5.34 %, N = 5.45 %, S = 13.58 %

1.2.3 4'-(Propylthio)-[1,1'-biphenyl]-4-carbonitrile (3SCB)

Yield: 0.500 g, 56.7 %. RF: 0.41

T_{Cr-} 63 °C T_{NI} (17 °C)

ν_{max}/cm^{-1}: 2964, 2925, 2230, 1606, 1483, 1456, 1434, 1391, 1291, 1277, 1180, 1094, 1000, 855, 845, 808, 732, 561, 550, 521

δ_H/ppm (400 MHz, $CDCl_3$): 7.71 (2 H, d, J 8.1 Hz, Ar-H), 7.65 (2 H, d, J 8.1 Hz, Ar-H), 7.50 (2 H, d, J 7.8 Hz, Ar-H), 7.39 (2 H, d, J 7.8 Hz, Ar-H), 2.96 (2 H, t, J 7.3 Hz, S-$\underline{CH_2}$-CH_2-), 1.72 (2 H, sext, J 7.3 Hz, S-CH_2-$\underline{CH_2}$-CH_3), 1.05 (3 H, t, J 7.3 Hz, S-CH_2-CH_2-$\underline{CH_3}$)

δ_C/ppm (100 MHz, $CDCl_3$): 144.95, 138.54, 136.08, 132.64, 128.68, 127.49, 127.33, 118.95, 110.76, 35.07, 22.44, 13.49

Elemental Analysis: Calculated for $C_{16}H_{15}NS$: C = 75.85 %, H = 5.97 %, N = 5.53 %, S = 12.65 %; Found: C = 75.92 %, H = 5.92 %, N = 5.12 %, S = 12.67 %

1.2.4 4'-(Butylthio)-[1,1'-biphenyl]-4-carbonitrile (4SCB)

Yield: 0.456 g, 49.1 %. RF: 0.46

T_{Cr-} 64 °C T_{NI} (36 °C)

ν_{max}/cm^{-1}: 2958, 2871, 2228, 1594, 1485, 1463, 1433, 1396, 1272, 1184, 1097, 1000, 848, 810, 747, 729, 559, 519, 456

δ_H/ppm (400 MHz, $CDCl_3$): 7.72 (2 H, d, J 8.1 Hz, Ar-H), 7.66 (2 H, d, J 8.1 Hz, Ar-H), 7.51 (2 H, d, J 8.0 Hz, Ar-H), 7.39 (2 H, d, J 8.0 Hz, Ar-H), 2.99 (2 H, t, J 7.5 Hz, S-$\underline{CH_2}$-CH_2-), 1.68 (2 H, quin, J 7.5 Hz, S-CH_2-$\underline{CH_2}$-CH_2-), 1.47 (2 H, m, S-CH_2-CH_2-$\underline{CH_2}$-CH_3), 0.95 (3 H, t, J 7.3 Hz, S-CH_2-CH_2-CH_2-$\underline{CH_3}$)

δ_C/ppm (100 MHz, $CDCl_3$): 144.93, 138.66, 136.01, 132.64, 128.54, 127.49, 127.32, 118.96, 110.74, 32.72, 31.10, 22.03, 13.68

Elemental Analysis: Calculated for $C_{17}H_{17}NS$: C = 76.36 %, H = 6.41 %, N = 5.24 %, S = 11.99 %; Found: C = 76.43 %, H = 6.29 %, N = 4.91 %, S = 11.71 %

1.2.5 4'-(Pentylthio)-[1,1'-biphenyl]-4-carbonitrile (5SCB)

Yield: 0.469 g, 39.3 %. RF: 0.48

T_{Cr} 55 °C T_{NI} (27 °C)

ν_{max}/cm^{-1}: 2955, 2925, 2856, 2234, 1591, 1484, 1464, 1396, 1186, 1099, 1001, 848, 808, 725, 558, 519, 474

δ_H/ppm (400 MHz, $CDCl_3$): 7.71 (2 H, d, J 8.0 Hz, Ar-H), 7.66 (2 H, d, J 8.0 Hz, Ar-H), 7.50 (2 H, d, J 7.8 Hz, Ar-H), 7.39 (2 H, d, J 7.8 Hz, Ar-H), 2.97 (2 H, t, J 7.5 Hz, S-$\underline{CH_2}$-CH_2-), 1.69 (2 H, quin, J 7.5 Hz, S-CH_2-$\underline{CH_2}$-CH_2-), 1.40 (4 H, m , S-CH_2-CH_2-$\underline{CH_2}$-$\underline{CH_2}$-CH_3), 0.91 (3 H, t, J 7.0 Hz, S-CH_2-CH_2-CH_2-CH_2-$\underline{CH_3}$)

δ_C/ppm (100 MHz, $CDCl_3$): 144.97, 138.64, 136.05, 132.64, 128.56, 127.49, 127.33, 118.95, 110.76, 33.03, 31.05, 28.73, 22.27, 13.98

Elemental Analysis: Calculated for $C_{18}H_{19}NS$: C = 76.82 %, H = 6.81 %, N = 4.98 %, S = 11.39 %; Found: C = 77.12 %, H = 6.74 %, N = 4.66 %, S = 11.27 %

1.2.6 4'-(Hexylthio)-[1,1'-biphenyl]-4-carbonitrile (6SCB)

Yield: 0.180 g, 45.4 %. RF: 0.43

T_{Cr} 63 °C T_{NI} (43 °C)

ν_{max}/cm^{-1}: 2953, 2924, 2854, 2235, 1590, 1485, 1456, 1395, 1185, 1099, 1000, 849, 809, 723, 558, 519, 468

δ_H/ppm (400 MHz, $CDCl_3$): 7.72 (2 H, d, J 8.3 Hz, Ar-H), 7.66 (2 H, d, J 8.3 Hz, Ar-H), 7.51 (2 H, d, J 8.3 Hz, Ar-H), 7.39 (2 H, d, J 8.3 Hz, Ar-H), 2.97 (2 H, t, J 7.4 Hz, S-$\underline{CH_2}$-CH_2-), 1.69 (2 H, quin, J 7.4 Hz, S-CH_2-$\underline{CH_2}$-CH_2-), 1.46 (2 H, quin, J 7.4 Hz, S-CH_2-CH_2-$\underline{CH_2}$-CH_2-), 1.31 (4 H, m, S-CH_2-CH_2-CH_2-$\underline{CH_2}$-$\underline{CH_2}$-CH_3), 0.89 (3 H, t, J 7.0 Hz, S-CH_2-CH_2-CH_2-CH_2-CH_2-$\underline{CH_3}$)

δ_C/ppm (100 MHz, $CDCl_3$): 144.97, 138.65, 136.05, 132.64, 128.57, 127.49, 127.33, 118.95, 110.76, 33.06, 31.37, 29.00, 28.57, 22.55, 14.03

Elemental Analysis: Calculated for $C_{19}H_{21}NS$: C = 77.24 %, H = 7.16 %, N = 4.74 %, S = 10.85 %; Found: C = 77.66 %, H = 7.11 %, N = 4.37 %, S = 10.44 %

1.2.7 4'-(Heptylthio)-[1,1'-biphenyl]-4-carbonitrile (7SCB)

Yield: 0.318 g, 31.0 %. RF: 0.46

T_{Cr} 65 °C T_{SmAN} (37 °C) T_{NI} (39 °C)

ν_{max}/cm^{-1}: 2953, 2924, 2853, 2234, 1595, 1484, 1462, 1391, 1186, 1096, 1020, 1001, 849, 812, 733, 718, 562, 522, 457

δ_H/ppm (400 MHz, $CDCl_3$): 7.72 (2 H, d, J 7.9 Hz, Ar-H), 7.66 (2 H, d, J 7.9 Hz, Ar-H), 7.51 (2 H, d, J 7.6 Hz, Ar-H), 7.39 (2 H, d, J 7.6 Hz, Ar-H), 2.97 (2 H, t, J 7.3 Hz, S-$\underline{CH_2}$-CH_2-), 1.68 (2 H, quin, J 7.3 Hz, S-CH_2-$\underline{CH_2}$-CH_2-), 1.44 (2 H, quin, J 7.3 Hz, S-CH_2-CH_2-$\underline{CH_2}$-CH_2-), 1.27 (6 H, m, S-CH_2-CH_2-CH_2-$\underline{CH_2}$-$\underline{CH_2}$-$\underline{CH_2}$-CH_3), 0.88 (3 H, t, J 6.9 Hz, S-CH_2-CH_2-CH_2-CH_2-CH_2-CH_2-$\underline{CH_3}$)

δ_C/ppm (100 MHz, $CDCl_3$): 144.97, 138.66, 136.05, 132.64, 128.57, 127.49, 127.33, 118.95, 110.76, 33.06, 31.71, 29.04, 28.85 (2 x C), 22.60, 14.09

Elemental Analysis: Calculated for $C_{20}H_{23}NS$: C = 77.62 %, H = 7.49 %, N = 4.53 %, S = 10.36 %; Found: C = 77.49 %, H = 7.45 %, N = 4.22 %, S = 10.24 %

1.2.8 4'-(Octylthio)-[1,1'-biphenyl]-4-carbonitrile (8SCB)

Yield: 0.541 g, 50.4 %. RF: 0.49

T_{Cr-} 67 °C T_{SmAI} (49 °C)

ν_{max}/cm^{-1}: 2953, 2921, 2852, 2235, 1591, 1485, 1464, 1380, 1186, 1099, 1001, 849, 809, 722, 717, 558, 520

δ_H/ppm (400 MHz, $CDCl_3$): 7.71 (2 H, d, J 8.1 Hz, Ar-H), 7.66 (2 H, d, J 8.1 Hz, Ar-H), 7.50 (2 H, d, J 7.9 Hz, Ar-H), 7.39 (2 H, d, J 7.9 Hz, Ar-H), 2.97 (2 H, t, J 7.5 Hz, S-$\underline{CH_2}$-CH_2-), 1.69 (2 H, quin, J 7.5 Hz, S-CH_2-$\underline{CH_2}$-CH_2-), 1.45 (2 H, quin, J 7.5 Hz, S-CH_2-CH_2-$\underline{CH_2}$-CH_2-), 1.29 (8 H, m, S-CH_2-CH_2-CH_2-$\underline{CH_2}$-$\underline{CH_2}$-$\underline{CH_2}$-$\underline{CH_2}$-CH_3), 0.88 (3 H Hz, t, J 6.9, S-CH_2-CH_2-CH_2-CH_2-CH_2-CH_2-CH_2-$\underline{CH_3}$)

δ_C/ppm (100 MHz, $CDCl_3$): 144.97, 138.66, 136.05, 132.64, 128.57, 127.49, 127.33, 118.95, 110.76, 33.06, 31.80, 29.17, 29.14, 29.03, 28.89, 22.65, 14.11

Elemental Analysis: Calculated for $C_{21}H_{25}NS$: C = 77.97 %, H = 7.79 %, N = 4.33 %, S = 9.91 %; Found: C = 78.34 %, H = 7.74 %, N = 4.26 %, S = 9.57 %

1.2.9 4'-(Nonylthio)-[1,1'-biphenyl]-4-carbonitrile (9SCB)

Yield: 0.295 g, 25.0 %. RF: 0.51

T_{Cr-} 70 °C T_{SmAI} (54 °C)

ν_{max}/cm^{-1}: 2954, 2921, 2850, 2234, 1595, 1485, 1461, 1391, 1185, 1095, 1001, 849, 812, 728, 717, 561, 522

δ_H/ppm (400 MHz, $CDCl_3$): 7.71 (2 H, d, J 8.1 Hz, Ar-H), 7.66 (2 H, d, J 8.1 Hz, Ar-H), 7.50 (2 H, d, J 8.0 Hz, Ar-H), 7.39 (2 H, d, J 8.0 Hz, Ar-H), 2.97 (2 H, t, J 7.5 Hz, S-$\underline{CH_2}$-CH_2-), 1.69 (2 H, quin, J 7.5 Hz, S-CH_2-$\underline{CH_2}$-CH_2-), 1.44 (2 H, quin, J 7.5 Hz, S-CH_2-CH_2-$\underline{CH_2}$-CH_2-),

1.29 (10 H, m, S-CH_2-CH_2-CH_2-$\underline{CH_2}$-$\underline{CH_2}$-$\underline{CH_2}$-$\underline{CH_2}$-$\underline{CH_2}$-CH_3), 0.88 (3 H, t, J 6.8 Hz, S-CH_2-CH_2-CH_2-CH_2-CH_2-CH_2-CH_2-$\underline{CH_3}$)

δ_C/ppm (100 MHz, $CDCl_3$): 144.97, 138.65, 136.05, 132.64, 128.57, 127.49, 127.33, 118.95, 110.76, 33.06, 31.87, 29.47, 29.25, 29.18, 29.03, 28.88, 22.67, 14.12

Elemental Analysis: Calculated for $C_{22}H_{27}NS$: C = 78.29 %, H = 8.06 %, N = 4.15 %, S = 9.50 %; Found: C = 78.46 %, H = 8.07 %, N = 3.92 %, S = 9.40 %

1.2.10 4'-(Decylthio)-[1,1'-biphenyl]-4-carbonitrile (10SCB)

Yield: 0.517 g, 40.4 %. RF: 0.45

T_{Cr-} 74 °C T_{SmAI} (58 °C)

ν_{max}/cm^{-1}: 2955, 2919, 2851, 2235, 1608, 1595, 1485, 1460, 1391, 1186, 1095, 1021, 1000, 849, 813, 734, 717, 562, 522

δ_H/ppm (400 MHz, $CDCl_3$): 7.71 (2 H, d, J 8.2 Hz, Ar-H), 7.66 (2 H, d, J 8.2 Hz, Ar-H), 7.50 (2 H, d, J 7.8 Hz, Ar-H), 7.39 (2 H, d, J 7.8 Hz, Ar-H), 2.97 (2 H, t, J 7.5 Hz, S-$\underline{CH_2}$-CH_2-), 1.69 (2 H, quin, J 7.5 Hz, S-CH_2-$\underline{CH_2}$-CH_2-), 1.44 (2 H, quin, J 7.5 Hz, S-CH_2-CH_2-$\underline{CH_2}$-CH_2-), 1.27 (12 H, m, S-CH_2-CH_2-CH_2-$\underline{CH_2}$-$\underline{CH_2}$-$\underline{CH_2}$-$\underline{CH_2}$-$\underline{CH_2}$-CH_3), 0.88 (3 H, t, J 7.0 Hz, S-CH_2-CH_2-CH_2-CH_2-CH_2-CH_2-CH_2-CH_2-$\underline{CH_3}$)

δ_C/ppm (100 MHz, $CDCl_3$): 144.97, 138.66, 136.04, 132.64, 128.57, 127.49, 127.32, 118.95, 110.76, 33.06, 31.90, 29.55, 29.51, 29.31, 29.18, 29.03, 28.88, 22.69, 14.13.

Elemental Analysis: Calculated for $C_{23}H_{29}NS$: C = 78.58 %, H = 8.32 %, N = 3.98 %, S = 9.12 %; Found: C = 78.93 %, H = 8.33 %, N = 3.78 %, S = 9.06 %

1.2.11 4'-(Undecylthio)-[1,1'-biphenyl]-4-carbonitrile (11SCB)

Yield: 0.322 g, 21.6 %. RF: 0.47

T_{Cr-} 78 °C T_{SmAI} (62 °C)

ν_{max}/cm^{-1}: 2953, 2918, 2849, 2234, 1595, 1484, 1460, 1391, 1186, 1095, 1000, 849, 812, 730, 717, 562, 522, 456

δ_H/ppm (400 MHz, $CDCl_3$): 7.72 (2 H, d, J 8.0 Hz, Ar-H), 7.66 (2 H, d, J 8.0 Hz, Ar-H), 7.50 (2 H, d, J 7.6 Hz, Ar-H), 7.39 (2 H, d, J 7.6 Hz, Ar-H), 2.97 (2 H, t, J 7.5 Hz, S-$\underline{CH_2}$-CH_2-), 1.69 (2 H, quin, J 7.5 Hz, S-CH_2-$\underline{CH_2}$-CH_2-), 1.44 (2 H, quin, J 7.5 Hz, S-CH_2-CH_2-$\underline{CH_2}$-CH_2-), 1.27 (14 H, m, S-CH_2-CH_2-CH_2-$\underline{CH_2}$-$\underline{CH_2}$-$\underline{CH_2}$-$\underline{CH_2}$-$\underline{CH_2}$-$\underline{CH_2}$-CH_3), 0.88 (3 H, t, J 7.1 Hz, S-CH_2-CH_2-CH_2-CH_2-CH_2-CH_2-CH_2-CH_2-CH_2-CH_2-$\underline{CH_3}$)

δ_C/ppm (100 MHz, $CDCl_3$): 144.97, 138.65, 136.04, 132.64, 128.57, 127.49, 127.32, 118.95, 110.76, 33.06, 31.91, 29.61, 29.59, 29.51, 29.34, 29.18, 29.03, 28.88, 22.69, 14.13

Elemental Analysis: Calculated for $C_{24}H_{31}NS$: C = 78.85 %, H = 8.55 %, N = 3.83 %, S = 8.77 %; Found: C = 78.57 %, H = 8.47 %, N = 3.61 %, S = 8.39 %

2.0 Phase Diagrams

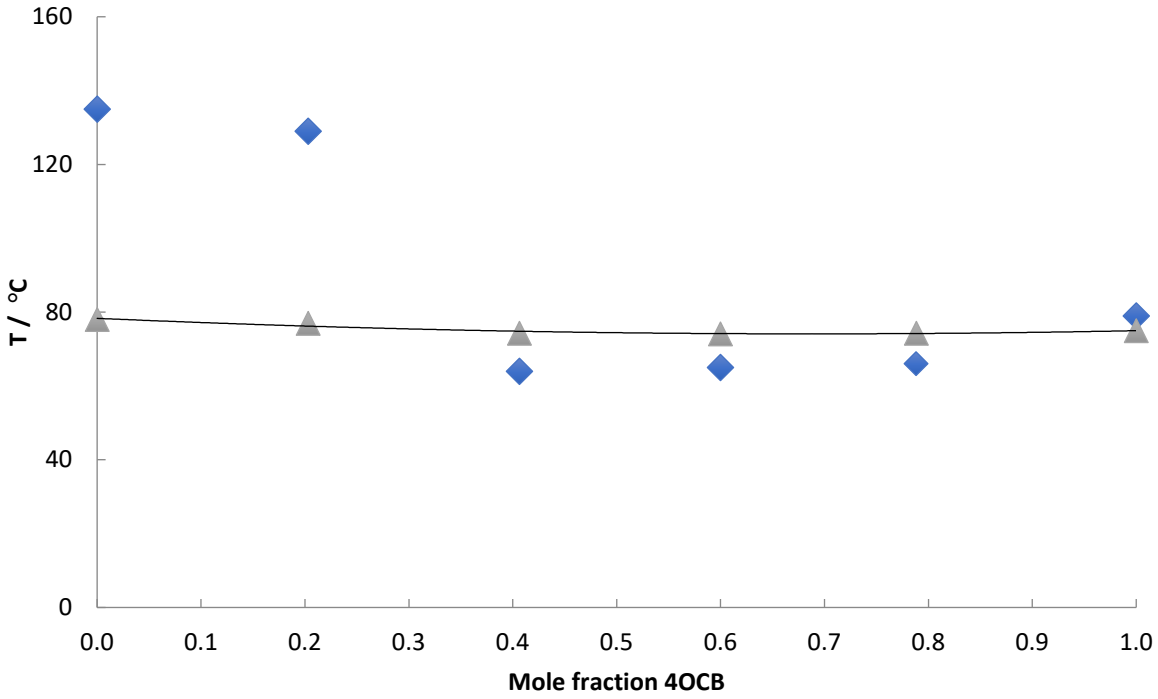

Figure SI1. Phase diagram constructed for binary mixtures of 1SCB and 4OCB. The triangles denote nematic-isotropic transitions with the solid line indicating the trendline for the nematic-isotropic transition temperatures. The diamonds indicate the melting points.

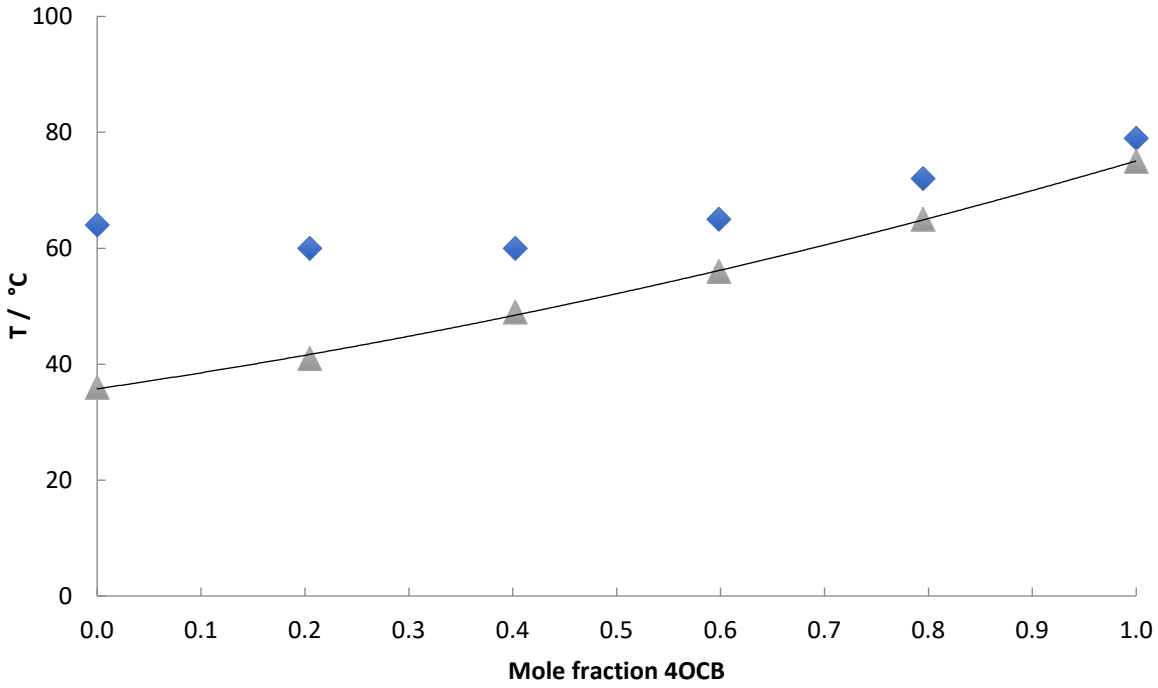

Figure SI2. Phase diagram constructed for binary mixtures of 4SCB and 4OCB. The triangles denote nematic-isotropic transitions with the solid line indicating the trendline for the nematic-isotropic transition temperatures. The diamonds indicate the melting points.

3.0 References

1. Semple, G., Santora, V. J., Smith, J. M., Covel, J. A., Hayashi, R., Gallardo, C., Ibarra, J. B., Schultz, J. A., Park, D. M., Estrada, S. A., Hofilena, B. J., Smith, B. M., Ren, A., Suarez, M., Frazer, J., Edwards, J. E., Hart, R., Hauser, E. K., Lorea, J. & Grottick, A. J. Identification of biaryl sulfone derivatives as antagonists of the histamine H 3 receptor: Discovery of (R)-1-(2-(4'-(3- methoxypropylsulfonyl)biphenyl-4-yl)ethyl)-2-methylpyrrolidine (APD916). *Bioorganic Med. Chem. Lett.* **22**, 71–75 (2012).
2. Yang, S., Xie, W., Zhou, H., Wu, C., Yang, Y., Niu, J., Yang, W. & Xu, J. Alkoxylation reactions of aryl halides catalyzed by magnetic copper ferrite. *Tetrahedron*. **69**, 3415–3418 (2013).